Bremsstrahlung from thick targets and a diagnostic for electron energy distributions

M. Lamoureux,* P. Waller,† P. Charles, and N. B. Avdonina‡
Laboratoire de Dynamique des Ions, Atomes et Molécules, C75, Université Pierre et Marie Curie, 4 Place Jussieu, 75252 Paris Cedex 05, France

(Received 28 September 1999; revised manuscript received 2 March 2000)

The bremsstrahlung from solid material caused by runaway electrons may blur severely the bremsstrahlung that is recorded from gases or plasmas in order to determine the energy distribution of their hot electrons. The expressions for these emissions are presented in order to compare their characteristics. Explanations are then given for an irregular feature observed at the tip of the spectrum for solid targets. More importantly, a type of diagnostics of energy distribution functions is proposed, based on analysis of the bremsstrahlung emissivity from thick targets. It can be implemented on experimental setups by purposely inserting a well-defined solid target into the electron trajectories, and it is applied as an example to the electron beam of microwave tubes. These diagnostics could also be taken advantage of to study runaway electrons hitting vessel walls.

PACS number(s): 78.70.Ck, 52.70.−m, 52.25.−b, 41.50.+h

I. INTRODUCTION

Bremsstrahlung (BR) from a plasma is routinely used to deduce the temperature of Maxwellian plasmas or the energy distribution of non-Maxwellian hot electrons (e.g., Refs. [1], [2]). Since accurate BR atomic cross sections are available, the precision of the diagnostics greatly depends on the quality of the experimental data. A current difficulty in this area is to avoid recording spurious emission from the walls of the experimental system. Severe collimations are often delicate to perform and of course do not provide any information on the runaway electrons. In Sec. II, the expressions are given for thin-target BR (gases and optically thin plasmas) and for thick-target BR, in which case an unexpected change of slope observed at the tip of the spectrum is explained. In Sec. III we show that thick-target BR can be turned into an advantage. The electron distribution diagnostics proposed in Eq. (10) below are as general and nearly as simple as the traditional type [Eq. (9)] based on the analysis of thin-target BR. As an example, these diagnostics are briefly applied to the electron beam of a microwave tube.

II. ELECTRON BREMSSTRAHLUNG FROM AN ATOM, A PLASMA, AND A THICK TARGET, AND STUDY OF THE TIP REGION FOR THICK TARGETS

Electron BR emissivities at the photon energy $h\nu$ are recalled for three physical situations in order to compare them quantitatively. For simplicity of presentation, they are given in the nonrelativistic regime. They all involve the cross section relative to the scattering of electrons of energy E by an atom or ion of atomic number Z. The general expression for the cross section is $d\sigma(E,h\nu)/dh\nu = (mc^2/2)(Z^2/E\,h\nu)\sigma_{\mathrm{Kr}}G(E,h\nu)$, where σ_{Kr} is the Kramers [3] cross section for H^+, that is $\sigma_{\mathrm{Kr}}=(16\pi\alpha^3/3\sqrt{3})\alpha^2 a_0^2$ for 4π sr. The Gaunt factor $G(E,h\nu)$ accounts for quantum, screening, and relativistic effects. The energy radiated will be labeled $j(h\nu)$ or $J(h\nu)$, depending on whether the incident electrons are monoenergetic or not. This emissivity is equal to the number of photons emitted, $N(h\nu)$, multiplied by the photon energy. At small $h\nu$, the number of photons actually recorded becomes significantly smaller than $N(h\nu)$ because of an increasing absorption coefficient $T(h\nu)$. This absorption is due to the windows (chamber and detector), the air between the windows, or the solid target itself. General recommendations on how to record the spectra and how to obtain the normalized value of $J(E,h\nu)$ from them are presented, e.g., in Ref. [4].

The energy radiated per unit energy interval per electron traveling over a distance Δz is equal to

$$j_{\mathrm{at}}(E,h\nu)=\frac{mc^2}{2}N_{\mathrm{at}}\frac{Z^2}{E}\sigma_{\mathrm{Kr}}G(E,h\nu)\,\Delta z, \tag{1}$$

where N_{at} is the atom or ion population density of a thin target (gas or plasma) with atomic number Z. This quantity is dimensionless (per electron). Coming now to a plasma, the BR is due to a variety of electrons distributed on $g(E)$, the electron distribution function (EDF). For a plasma with ionic density N_i, ionic atomic number Z_i, and electron density N_e, the energy radiated by unit energy interval per unit of time in the volume ΔV is

$$J_{\mathrm{pl}}(h\nu)=\frac{mc^2}{2}N_iN_eZ_i^2\sigma_{\mathrm{Kr}}\left(\int_{h\nu}^{\infty}\frac{1}{E}vg(E)G(E,h\nu)dE\right)\Delta V \tag{2}$$

and the dimension here is the inverse of time. Finally, when the electrons of a monoenergetic beam impinge upon a solid target, they are slowed down inside the solid of atomic number Z_{sol} and atomic density N_{sol}, so that the emission accumulated over time comes in fact from electrons having various energies. This is taken into account in the stopping power dE/dz through the expression

*Electronic address: mla@ccr.jussieu.fr
†Also at Thomson-Tubes Electroniques, 2 rue Latécoère BP23, 78141, Vélizy-Villacoublay Cedex, France.
‡Present address: Department of Physics, University of Pittsburgh, Pittsburgh, PA 15260.

 ©2000 The American Physical Society

$$j_{\mathrm{sol}}(E,h\nu)=\frac{mc^2}{2}Z_{\mathrm{sol}}^2\sigma_{\mathrm{Kr}}N_{\mathrm{sol}}\int_{h\nu}^{E}\frac{1}{E}\frac{G(E,h\nu)}{dE/dz}dE. \quad (3)$$

This third quantity is again dimensionless (per electron).

Simple estimates for the emissivity coefficients are obtained by using Gaunt factors equal to unity, the Maxwellian EDF, and the Kramers stopping power [3], which is itself proportional to N_{sol}. Equations (1)–(3) become the following, when distances and volumes are expressed in SI units but the energies and the temperature in keV.

$$j_{\mathrm{at}}(E,h\nu)=(1.43\times10^{-28})N_{\mathrm{at}}\frac{Z^2}{E}\Delta z \quad \text{per electron,} \quad (4)$$

$$J_{\mathrm{pl}}(h\nu)=(3.0\times10^{-21})N_iN_eZ_i^2\frac{1}{\sqrt{kT}}\exp\left(-\frac{h\nu}{kT}\right)\Delta V \quad \text{per s,} \quad (5)$$

$$j_{\mathrm{sol}}(E,h\nu)=(1.10\times10^{-5})\frac{Z_{\mathrm{sol}}}{l}(E-h\nu) \quad \text{per electron.} \quad (6)$$

The comparative characteristics of these three types of emission are displayed in Fig. 1, and are globally confirmed by more elaborate calculations. For monoenergetic electrons, the BR energy radiated by a thin target is independent of $h\nu$ and proportional to N_{at}. On the contrary, the energy radiated by a thick target increases with decreasing $h\nu$ and is independent of N_{sol}. Because of this point and of the largest numerical factor in Eq. (6), the parasite emission coming from walls easily dominates the core continuum emission when the gas or the plasma is not dense enough. In order to solve that problem, the next section will propose diagnostics for the EDF based on thick-target BR. This solid target may stand in the way of the electrons naturally, or can be purposely inserted into their way in order to make this emission dominant. Just as the $1/E$ dependence is at the basis of the temperature determination in Eq. (5), the $(E-h\nu)$ dependence will be essential for these diagnostics, and is therefore probed before further development.

Elaborate calculations and a test experiment involving monoenergetic beams have been carried out in relation to the study of microwave tubes (see Sec. III), that is, for energies of a few keV. Calculations using accurate Coulomb or screened BR cross sections [5] and a more precise stopping power confirm the $(E-h\nu)$ law in the energy region involved. In the test experiment, the Be target used in Sec. III intercepts a monoenergetic electron beam, and the emission is recorded by a high resolution SiLi detector. For $T(h\nu)$, a Gaussian average (with $\sigma=64$ eV) was used in order to take into account the resolution of the detector and to smooth out the K edge of the Kr impurity in air. The calculated BR intensity agrees with the experimental one within the precision at which the viewing solid angle is estimated, i.e., within a few percent. However, looking closely at the experimental spectrum in Fig. 2, a steeper descent than expected is noticed in the end region of the spectrum. The $(E-h\nu)$ dependence predicted by Eq. (6) is not strictly followed, as we observe

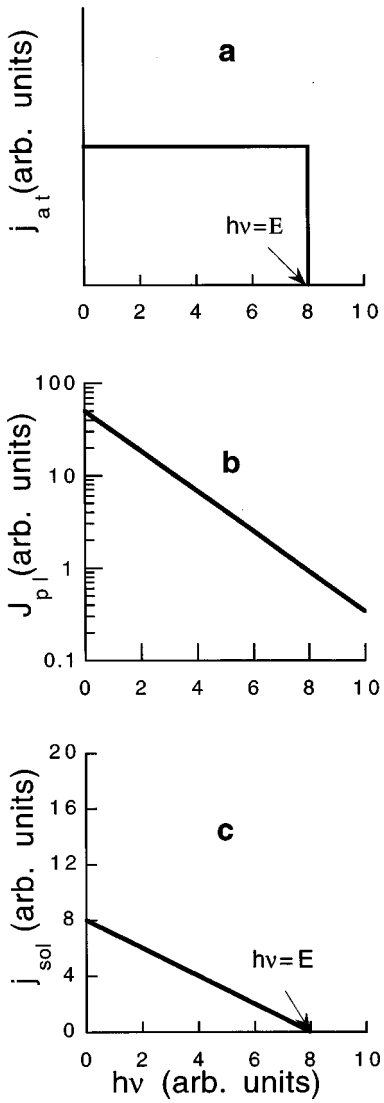

FIG. 1. Schematic view of electron bremsstrahlung emissivities (energy radiated), obtained in the simple approaches described in the text, versus the photon energy $h\nu$: (a) thin-target BR for electrons of energy E [Eq. (4)]; (b) BR from a Maxwellian plasma [Eq. (5)]; (c) thick-target BR for electrons of energy E [Eq. (6)].

$$j_{\mathrm{sol}}(E,h\nu)\propto(E-h\nu+E_s) \quad \text{for } h\nu<E\text{-}\Delta E. \quad (7)$$

A similar behavior was noted many years ago [6,7] for heavier materials and larger energies. To our knowledge, it has never been explained.

The steeper descent at the tip is attributed in this experiment to the presence of impurities (mostly Cu, Fe, Al, Si, and C) on top of the Be target, as revealed by an electron microscope impurity analysis. This is coherent with the fact that an impurity with $Z_i>Z_{\mathrm{sol}}$ in Eq. (6) leads to a stronger slope at the tip of the spectrum and to a shift E_s for the rest of it. This is illustrated in Fig. 3(a). The shift E_s and the value ΔE went over to the stable value of 0.40 keV shortly after the beginning of the experimental runs, which shows that the impurities had been released during the baking stage of tube manufacture. As a confirmation, a duplicate target, never inserted into the tube but only into the electron microscope chamber, leads to a shift of only about 0.14 keV, which can then be ascribed mostly to O and Si impurities.

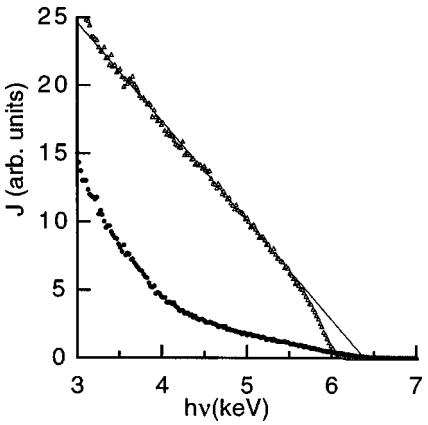

FIG. 2. Experimental thick-target BR emissivity $J_{sol}(h\nu)$ versus photon energy for the initially monoenergetic beam of 6.0 keV (top, triangles), and for the beam after its interaction with a 12.75 GHz microwave (bottom, circles).

Coming back to the earlier results of Refs. [6,7], the above interpretation involving impurities is evidently not appropriate when Pt and Au targets are involved. For these cases, the emission on top of the standard $(E-h\nu)$ quantity might be due to the direct radiative recombination of electrons into the ionized atoms of the target. Important ionization can indeed be produced by large current densities [8]. For electrons recombining into the n shell of A^{q+} ions, the cumulated emission becomes $[E-h\nu+\alpha^2(mc^2)q^4/Z^2n^3]$. For a fully ionized Be target, this leads to a shift $E_s = 0.43$ keV, which confirms that impurities undoubtedly play a role in our case. Analyses of the shifts of Ref. [7] show that they correspond to stable configurations of the ions, which supports this second interpretation. The spectrum calculated for the successive ionizations of Be is shown in Fig. 3(b). The overall decrease would be smoothed out partly by the detector's resolution. In conclusion, the spectra simulated by the two different interpretations equally reproduce the shape shown in Fig. 2 for the monoenergetic beam.

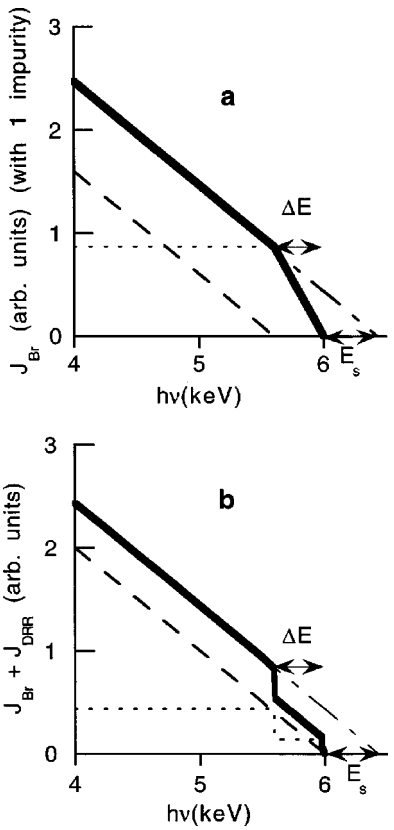

FIG. 3. Schematic view of the composite continuum spectrum (solid line). The standard BR emissivity (long dashes) from the Be target receives an additional contribution (short dashes) (a) from the BR from a heavy impurity layer and (b) from direct radiative recombination into ionized Be.

In practice, it is not necessary to identify the detailed causes of the eventual steeper descent in the tip region. It is sufficient to measure the characteristics E_s and ΔE with the help of monoenergetic beams, before proceeding to the investigation of nonmonoenergetic distributions.

III. DIAGNOSTICS OF THE ENERGY DISTRIBUTION FUNCTION

For a nonmonoenergetic beam, the continuum emission observed per unit of time involves the product of the EDF with the velocity of the electron v, that is, $vg(E)$, or in other words a quantity proportional to the current reaching the target. In general, the proportion of current carried by electrons of energy larger than E is labeled $I(E)/I_0$. This quantity and the BR emissivity are given by

$$I(E)/I_0 = \int_E^\infty vg(E)dE$$

and

$$J(h\nu) = \int_{h\nu}^\infty j(E,h\nu)vg(E)dE. \tag{8}$$

The retarding tension method consists in directly measuring $I(E)$ with a probe, which immediately provides the EDF. Unfortunately, the experiment perturbs the region diagnosed, especially for large E, when many electrons are thrown back into it. In contrast, BR measurements have the great advantage of being passive. Depending on whether the electrons are scattered by a thin or by a thick target, Eq. (4) or Eq. (6) has to be used for $j(E,h\nu)$ in Eq. (8). Leaving aside for simplicity the straightforward numerical constants, this leads for thin targets to the well-known determination of the EDF [1]:

$$g(E) \propto \sqrt{E}\left.\frac{dJ_{\text{at or pl}}(h\nu)}{dh\nu}\right|_{h\nu=E}. \tag{9}$$

In the case of thick targets, the photon spectra have not been exploited beyond the fact that the terminal points in a spectrum at $h\nu_{max}$ indicate the presence of runaway electrons of energy $E_{max}=h\nu_{max}$ [1]. Insertable probes have been used in a few cases [9], but only the total power radiated P was studied. The $(E-h\nu)$ behavior of Eq. (6) was also assumed in these studies. The two parameters of a presupposed bi-Maxwellian distribution, and/or the drift velocity, were then determined from P. Taking advantage of Eqs. (6) and (8), a more general type of diagnostics is here established from

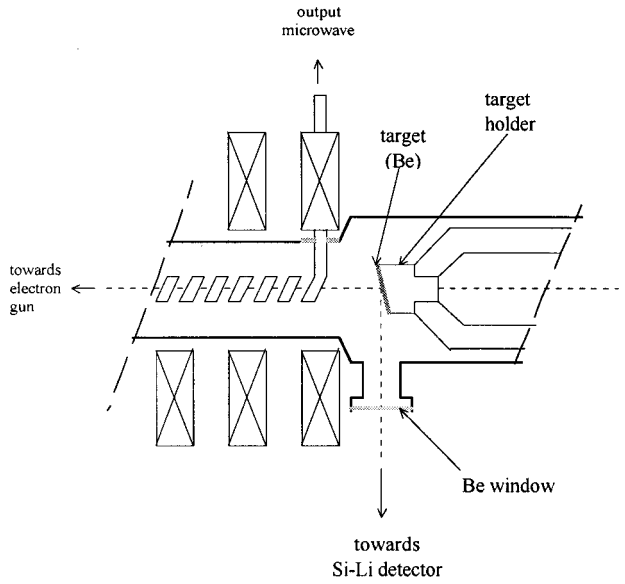

FIG. 4. Experimental setup showing the end region of the microwave tube. The photons were recorded perpendicularly to the electron beam impinging on the inserted target, by a Si-Li detector located behind the lateral beryllium window. The distance of air between the two beryllium windows (tube and detector) is 11 cm. In order not to saturate the detector, a severe collimation was enforced.

analysis of the detailed photon energy spectrum itself, and it does not require any preliminary notion about the shape of the EDF. These simple diagnostics are

$$\sqrt{E}g(E)\propto\left.\frac{d^2J_{\mathrm{sol}}(h\nu)}{d^2h\nu}\right|_{h\nu=E}\quad\text{and}\quad I(E)\propto-\left.\frac{dJ_{\mathrm{sol}}(h\nu)}{dh\nu}\right|_{h\nu=E}. \tag{10}$$

In situations where the spectra relative to monoenergetic beams exhibit a shift E_s, these expressions remain valid only when $h\nu$ or $E>E_{\max}-\Delta E$. In this outer region, the emission comes exclusively from the outside part of the target, which, depending on the interpretation of E_s, contains the impurity layer or is only slightly ionized. In the central and dominant part of the spectrum, the emission comes also from the inner region of the target, and the diagnostics take a slightly more complicated expression. The ratio $\Delta E/(\Delta E+E_s)=c/c_i$ has to be determined empirically in a preliminary step. Notice that when a coat consisting of one impurity covers the target, the values c and c_i reduce to the proportionality constants in Eq. (6), and $c/c_i=Z_{\mathrm{sol}}/Z_i$. For $h\nu<E_{\max}-\Delta E$, we have

$$\sqrt{E}g(E)\propto\frac{1}{c_i}\left.\frac{d^2J_{\mathrm{sol}}(h\nu)}{d^2h\nu}\right|_{h\nu=E}+\left(1-\frac{c}{c_i}\right)\sqrt{E+\Delta E}g(E+\Delta E), \tag{11a}$$

$$I(E)\propto-\frac{1}{c_i}\left.\frac{dJ(h\nu)}{dh\nu}\right|_{h\nu=E}+\left(1-\frac{c}{c_i}\right)I(E+\Delta E). \tag{11b}$$

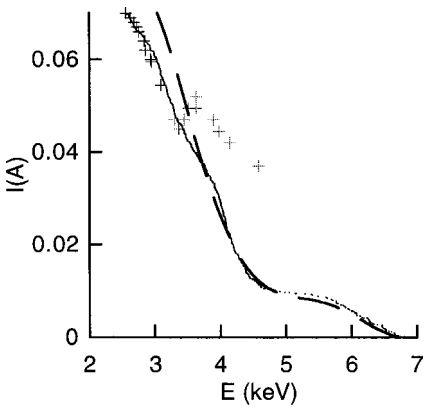

FIG. 5. Comparisons of $I(E)$ curves obtained for the electron beam initially at 6 keV after its interaction with the 12.75 GHz microwave. (Dashed curve) determined from the BR spectrum through Eqs. (10) and (11); + data points measured by the retarding tension method and valid only at small energies; dotted curve, numerical results by the 2.5D code [11].

Unlike in Eq. (10), the results do not depend only on the local derivatives, but can be determined inward from the end of the spectrum. In our example, E_s and ΔE are similar, that is, $c_i=2c$, which leads to

$$\sqrt{E_{\max}-n\Delta E}g(E_{\max}-n\Delta E)\propto J''_{\mathrm{sol}}(E_{\max}-n\Delta E)+\sum_{q=2}^{n}\frac{1}{2^{q-1}}J''_{\mathrm{sol}}[E_{\max}-n\Delta E+(q-1)\Delta E], \tag{12}$$

where the first term on the right-hand side corresponds to the simpler determination by Eq. (10).

As an example, the diagnostics are applied to microwave tubes. In such tubes [10], a monoenergetic beam launched by an electron gun is slowed down by the interaction with a microwave that thereby gets amplified. The tube studied was manufactured by Thomson Tubes Electroniques. It is dedicated to spatial communications, so that it is important to reduce the weight and increase the durability. This optimization requires precise data on the electron beam beyond the interaction zone, as these are important for improved design of the industrial multigrid electron collector. Various codes are available in one dimension (1D), and a 2.5 D code has recently been written [11]. It predicts that the electrons originally at 6 keV are spread out in the range 2.5–7 keV, with a majority of them at around 4 keV. In order to test these codes, experimental data on the EDF are desirable. The only ones available at present are meaningful only to about 3 keV because of the shortcomings of the retarding tension method. Another type of experiment was thus needed to cover the higher electron energies. For that purpose, a BR experiment was implemented on the tube. A window was laterally installed at the end of the interaction region in order to record the continuum spectrum. A SiLi detector was located 11 cm behind it, as illustrated in Fig. 4. The residual gas density in the tube is estimated at 10^{13} atoms cm^{-3}. According to Eqs. (4) and (6), even a very tiny fraction of badly collimated electrons hitting the wall would make the BR emission from

the gas negligible. For that reason, a solid target was located in the path of the electron beam (see Fig. 4), and the thick-target BR analyzed.

The emissivity curve deduced from the photon spectrum is given in Fig. 2. It lies lower than in the case of the monoenergetic beam, as expected, since most electrons are slowed down. The emission looks as if caused by a primary beam at about 3.5 keV and a secondary one at about 6.6 keV. This is confirmed by the $I(E)$ results deduced from Eqs. (10)–(11) and given in Fig. 5. The few data points obtained by the retarding tension method are also plotted. Evidently, $I(E)$ in Eq. (8) is a monotonically decreasing function, and, as expected from this method, only the points at the lower energies are acceptable. On the other hand, the $I(E)$ curve deduced from the BR spectrum loses precision at small energies (starting below around 3.0 keV) because of increasing photon absorption. The validity domains of these two sets of experiments are thus complementary, as desired. Within the restrictions expressed for each of them, the two sets of experimental results are coherent with each other.

Figure 5 compares the experimental results with the numerical ones obtained by the 2.5D code. The values provided by the 1D code are not given for clarity, but lie about 1 keV on the right side of the present cluster of curves. The description of these codes does not lie within the scope of this work, but can be found elsewhere [11]. In the 2.5D code, the increase of the electron beam size and the electron-wave interaction are treated self-consistently. The comparison with experimental data shows that this elaborate treatment is necessary and successful. As a secondary conclusion, it confirms the survival of electrons with energies close to the initial energy. Needless to say, the wave amplification is also much better reproduced by the 2.5D code [11].

In conclusion, diagnostics based on the analysis of thick-target BR proved helpful to investigate the wave-electron interaction in microwave tubes. The diagnostics are easy to use. The method could easily be applied to other types of beams, and also to the study of runaway electrons in plasmas.

ACKNOWLEDGMENTS

This work was supported in part by the Centre National d'Etudes Spatiales and Thomson-Tubes Electroniques. N.B.A. acknowledges a PECO grant from the French Ministère de l'Education Nationale de la Recherche et de la Technologie which supported her visit from Russia to the Université Pierre et Marie Curie, whose hospitality she appreciated. The authors are also very grateful to J. P. Briand and G. Giardino for very helpful discussions and encouragement.

[1] I. H. Hutchinson, *Principles of Plasma Diagnostics* (Cambridge University Press, Cambridge, England, 1992), Chap. 5.
[2] M. Lamoureux, Adv. At., Mol., Opt. Phys. **31**, 233 (1993), and references therein.
[3] H. A. Kramers, Philos. Mag. **46**, 836 (1923).
[4] C. A. Quarles, in *Accelerator-Based Atomic Physics Techniques and Applications*, edited by S. Shafroth and J. Austin (AIP, Woodbury, NY, 1997), Chap. 8.
[5] R. H. Pratt and I. J. Feng, in *Atomic Inner-Shell Physics*, edited by B. Craseman (Plenum, New York, 1985), and references therein; Lynn Kissel, C. A. Quarles, and R. H. Pratt, At. Data Nucl. Data Tables **28**, 381 (1983).
[6] N. A. Dyson, *X-Rays in Atomic and Nuclear Physics*, 2nd ed. (Cambridge University Press, Cambridge, England, 1990), Chap. 2.
[7] H. Kulenkampff, Ann. Phys. (Leipzig) **69**, 548 (1922).
[8] M. Stenke, K. Aichele, D. Hathiramani, G. Hofman, M. Steidl, R. Völpel, V. P. Shevelko, H. Tawara, and E. Salzborn, J. Phys. B **28**, 4853 (1995).
[9] Sam Hokin, Rev. Sci. Instrum. **63**, 5041 (1992); A. Welander and H. Bergsaker, Plasma Phys. Controlled Fusion **40**, 319 (1998).
[10] A. S. Gilmour, *Principles of Traveling-Wave Tubes* (Artech, Boston, 1994).
[11] P. Waller, Thèse d'université D. Diderot, Paris, 1999 (unpublished) (in French).